ACS APPLIED MATERIALS & INTERFACES

Research Article

www.acsami.org

Electrochemically Patterned Transducer with Anisotropic PEDOT through Liquid Crystalline Template Polymerization

Neethu Kalloor Sadanandhan, Sudha Janardhanan Devaki,* Rohini Kuttiplavil Narayanan, and Molji Cheriyathuchenaaramvalli

Chemical Science and Technology Division, CSIR-National Institute for Interdisciplinary Science and Technology, Thiruvananthapuram 695 019, India

Supporting Information

ABSTRACT: We have demonstrated patterning of highly ordered nanostructured conducting PEDOT (poly(3,4-ethylenedioxythiophene)) on glassy carbon electrode (GCE) through electrochemical polymerization of a biobased liquid crystalline template of EDOT-PDPPA (3-pentadecylphenyl phosphoric acid). Self-assembled "EDOT-PDPPA" in water exhibited lyotropic liquid crystalline (LC) phases of nematic gyroid, columnar, and lamellar phases. Studies revealed that, during electrochemical polymerization, PEDOT-PDPPA mimicked the anisotropic domains of its monomer LC template. Nyquist plot showed enhancement in conductivity with a positive change in the HOMO–LUMO gap. Further, the efficiency of the modified GCE was demonstrated as an electrochemical transducer for the detection of nicotine. It was observed that oxidation of nicotine occurs at lower potential (0.83 V) with higher current (54.63 μA) compared to bare GCE (1.1 V, 17.86 μA) with nanomolar detection. This simple strategy of electrochemical patterning of conductive polymer on a conventional electrode can be exploited for the high tech applications in miniaturized plastronic devices.

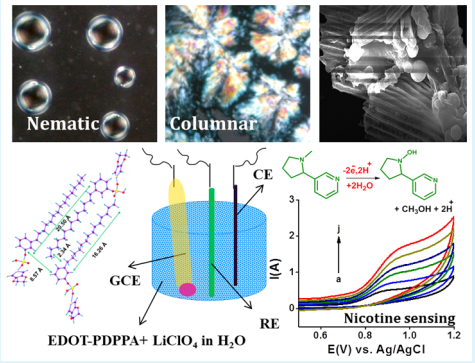

KEYWORDS: *electrochemical patterning, self-assembly, PEDOT, liquid crystal, square wave voltammetry, nicotine*

INTRODUCTION

Modification of electrodes using nanostructured conductive polymers (CPs) has received a lot of attention in both academia and industry, owing to their unique optical, electrical, and electrochemical properties and good environmental stability, which may find applications in the field of sensors, electrochromic devices, organic light emitting diodes, solar cells, drug delivery systems, actuators, etc.[1−4] Among the various CPs, PEDOT (poly(3,4-ethylenedioxythiophene)) has been identified as a reliable functional material for a wide range of applications because of its tunable conductivity by doping, high charge carrier mobility, optical transparency, low band gap, flexibility, ease of preparation, versatility for side chain functionalization, and bioconjugation.[5−9] But the control of the structure and orientation of PEDOT is limited due to its low solubility and infusibility. Several methods are adopted for improving or attaining a higher degree of molecular orientation, such as deposition of PEDOT in an oriented environment like Langmuir–Blodgett films.[10] However, these strategies lack in the prediction of morphology and performance.[11,12] Other promising strategies reported for the enhancement in the ordering of CPs are to prepare them in the nanometer regime using self-assembly. This can be carried out by the selective control of noncovalent interactions such as hydrogen bonding, van der Waals forces, $\pi-\pi$ stacking, and so forth.[13,14] The different synthetic routes include synthesis in micellar media,[15,16] template-guided polymerization using porous surfaces[17,18] and liquid crystalline (LC) phases.[19−21] Aqueous solutions containing a variety of anionic, cationic, or nonionic surfactants can self-assemble to form concentration dependent LC phases of specific textures.[22−25] These specific textures may contain well-organized channels which can be exploited to tune the size and shape of the functional nanomaterials. Stupp et al. studied the electrochemical polymerization of EDOT in a hexagonal lyotropic LC template and observed that formed PEDOT retained the texture and optical anisotropy of the LC template.[20] We have recently reported the preparation of water dispersible PEDOT nanospindles through chemical polymerization from the liquid crystalline phase of the spindle shaped smectic phase.[21] We have observed that the ordered molecular chains in the polymer imitated the anisotropic nature of the monomer. The shape and ordering of the liquid crystalline monomer are locked in PEDOT in the nanometer regime due to the thermodynamic influence of the growing chain.

Due to the hike in the price and scarcity for the petroleum based surfactants, now researchers are in search of low cost renewable resource based products. Among them, cashew nut shell liquid (CNSL) is receiving importance as an alternate source for unsaturated long chain phenols.[26] It is a low cost, abundantly available industrial byproduct obtained from the

Received: June 4, 2015
Accepted: July 22, 2015
Published: July 22, 2015

DOI: 10.1021/acsami.5b04916
ACS Appl. Mater. Interfaces 2015, 7, 18028−18037

cashew industry. The main constituent of CNSL is cardanol (3-pentadecenylphenol), which can be separated by a distillation process. 3-Pentadecylphenyl phosphoric acid, denoted as PDPPA, is a phosphoric acid derivative of cardanol. It has a unique built-in amphiphilic design consisting of a hydrophilic headgroup of phosphoric acid and a long alkyl chain as hydrophobic tail. Development of nanostructured conducting polymers using PDPPA as structure directing agent was reported earlier from our group.[27]

Electroanalytical techniques have received considerable attention in the area of sensors due to their quick response, relatively high sensitivity, the ability to be miniaturized, low cost for instrumentation, and suitability for real time detection. Voltammetry is used for studying current potential behavior. The current corresponding to the quantity of material transported by diffusion and reacting at the electrode surface is usually measured. Cyclic voltammetry is a potentiodynamic electrochemical measurement in which it scans the electric potential before turning to the reverse direction after reaching the final potential and then scans back to the initial potential. Square wave voltammetry (SWV) is an electroanalytical technique which amends the signal-to-noise ratio by subtracting most of the short time responses, such as double layer capacitance, and leaving most of the slower processes, like Faradaic features.[28] Nicotine is a neuroactive pyridine derivative alkaloid present in tobacco leaves. The continuous intake of nicotine may cause cancer in various organs, like the lungs, mouth, kidney, and pancreas, and also increase the heartbeats, blood pressure, coronary heart disease, and pulmonary disease, etc.[29] Despite its toxic effects, nicotine has many therapeutic applications in a variety of disorders, such as Parkinson's disease and Alzheimer's disease.[30−32] Consequently, the detection of nicotine is important in several areas, such as chemistry, toxicology, pharmacology, and clinical and environmental fields. The slow kinetics of nicotine makes it oxidize at very higher potentials at glassy carbon electrode (GCE). Novel electrode materials for the modification of GCE are receiving importance in the present scenario. Modification of GCE with well-defined nanostructured CP is increasing in interest due to its ability to detect and transduce chemical or physical information into an electrical signal.[6,33] Moreover CPs can efficiently adhere with the electrode and will be compatible with the aqueous and biological media.

In the present work, we are reporting the electrochemical patterning of conductive PEDOT on GCE using a liquid crystalline template formed from an adduct of EDOT-PDPPA. The liquid crystalline phase was characterized by PLM. The effect of the liquid crystalline phase on the morphology, HOMO−LUMO gap, and conductivity of the PEDOT were studied. Finally the efficiency of the modified GC electrode as a transducer for the detection of nicotine was demonstrated.

EXPERIMENTAL SECTION

Materials and Methods. 3-Pentadecylphenyl phosphoric acid was prepared from 3-pentadecyl phenol as per the reported procedure.[27] EDOT, nicotine, lithium perchlorate, potassiumferricyanide and potassium ferrocyanide were purchased from Sigma-Aldrich Chemicals Pvt. Ltd., India. All solutions were prepared in deionized water.

X-ray diffraction studies were done using powder X-ray diffractometer (Philips X'pert Pro, Netherlands) with CuKα radiation ($\lambda \sim 0.154$ nm) employing X'celarator detector and monochromator at the diffraction beam side. Thin films casted on glass plates were used employing standard sample holder. FT-IR measurements of the polymers were made using fully computerized Nicolet impact 400D FT-IR spectrophotometer (Czech Republic, EU). Critical micelle concentration studied by UV−vis spectrum. Polarized light micrographs (PLM) were taken in an Olympus BX 51 microscope after drop casting the solution of the sample in a clean dry glass plate. The SEM images were obtained with SEM/EDAX (Scanning Electron Microscopy, JEOL JSM 5600 LV. EDS., EDAX, NJ, USA).

Electrochemical experiments were carried out using CHI6211B Electrochemical Analyzer, in a three-electrode one-compartment electrochemical cell in which GCE served as working electrode and a platinum wire used as a counter electrode. All the potentials were recorded using Ag/AgCl as the reference electrode. Prior to electrochemical experiments, GCE was polished with 0.03 micron alumina and then ultrasonically cleaned for about 5 min in doubly distilled water. Finally, the electrode was washed thoroughly with double distilled water. All the experiments were carried out at 25 ± 5 °C. Before performing the experiments, the solution was purged with nitrogen gas for 10 min and current was passed. Electrochemical impedance measurements were carried out at a frequency range of 0.1 Hz to 10 kHz. To obtain EIS data, the modified Randle circuit consisting of solution resistance (R_s), electron transfer resistance (R_{ct}), constant phase element (CPE) and Warburg impedance (W) was used.

Preparation and Characterization of Liquid Crystalline Template, EDOT-PDPPA. EDOT-PDPPA was prepared by mixing the equimolar proportion of EDOT and PDPPA at room temperature for 30 min. Then it was dispersed in water by slow addition. Its critical micelle concentration was determined by measuring UV−vis absorption intensity by varying the concentrations of EDOT-PDPPA in water. From UV−visible spectroscopic data the CMC of EDOT-PDPPA was found out by taking the concentration corresponding to the inflection point in the absorbance vs concentration plot. Liquid crystalline behavior of EDOT-PDPPA was studied by observation under PLM.

Electrochemical Patterning of PEDOT on GCE. Electrochemical patterning of PEDOT on GCE was performed by electrochemical polymerization of liquid crystalline template of EDOT-PDPPA by cyclic voltammetry (CV). Experiments were performed in 0.1 M $LiClO_4$ aqueous solution containing EDOT-PDPPA of concentrations 10 mM (nematic), 20 mM (columnar) and 30 mM (lamellar). CVs were recorded in the potential range between −0.2 to 0.9 V at the scan rate 0.05 V/s for 15 cycles. PEDOT film was formed on the surface of the GCE during electrochemical polymerization EDOT-PDPPA. Later, it was scanned for 5 cycles in monomer free electrolyte to remove the unreacted monomer from the electrode. GCE patterned with PEDOT-PDPPA was taken for further characterization. Experiments were performed with liquid crystalline template of EDOT-PDPPA in nematic, columnar, lamellar phase and also a control experiment was carried out with EDOT alone. They were designated as NPEDOT, CPEDOT, LPEDOT and PEDOT for polymers prepared from LC phases of nematic, columnar, lamellar and control, respectively. LPEDOT modified GCE was used for studying the detection of nicotine.

Detection of Nicotine. Electrochemical detection of nicotine was carried out using LPEDOT/GCE in BR buffer (pH 8.0) in a potential range of 0.4 V to +1.2 V by CV and SWV. Parameters optimized for SWV are amplitude (0. 25 V), frequency (15 Hz) and sensitivity (0.001 V). Three brands of commercial cigarettes (C1 to C3) were purchased from local super market. From each brand 10 cigarettes were taken and tobaccos were collected separately and dried in an oven for 30 min at 40 °C and were grounded with a mortar and pestle. Tobacco powder (0.1 g) was placed in a 50 mL glass vial and 10 mL of deionized water was added and the vial was capped. The mixture was sonicated for 3 h in an ultrasonic water bath at room temperature and filtered. An aliquot (100 μL) of the clear filtrate of each sample was added to the cell containing 10 mL of BR buffer (pH 8.0) and measurements were made by square wave voltammetry.

DOI: 10.1021/acsami.5b04916
ACS Appl. Mater. Interfaces 2015, 7, 18028−18037

RESULTS AND DISCUSSION

Studies on the Formation of Adduct EDOT-PDPPA and Its Liquid Crystalline Phases. Polymerizable liquid crystalline adduct "EDOT-PDPPA" was prepared by mixing EDOT and PDPPA in equimolar proportion. The stability of the adduct "EDOT-PDPPA" was theoretically checked by energy minimization using Gaussian software with the B3LYP method with a basis set 6-31G and is shown in Figure 1A. The

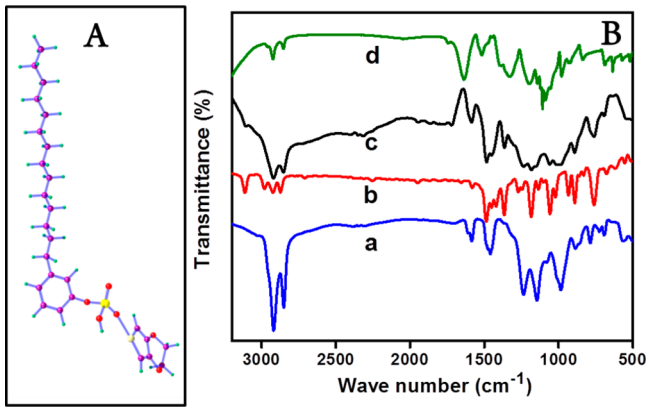

Figure 1. (A) Energy minimized structure of EDOT-PDPPA; (B) FTIR-spectra of (a) PDPPA, (b) EDOT, (c) EDOT-PDPPA, and (d) PEDOT-PDPPA.

observed higher negative value of the binding energy (−4.5 kcal) confirms the stability of the adduct "EDOT-PDPPA". The energy minimized structure of adduct "EDOT-PDPPA" showed a bent core structure suggesting its proclivity for the formation of self-assembled supramolecular liquid crystalline phases through various noncovalent interactions.[34] Studies also give insight into the charge transfer interaction between the thioether group of EDOT and the phosphoric acid group of PDPPA which leads to the adduct formation. Further, the charge transfer interaction and the formation of stable adduct "EDOT-PDPPA" were supported by the results obtained from the FTIR spectra. The FTIR spectra of EDOT, PDPPA, and EDOT-PDPPA are shown in Figure 1B. The characteristic band of P−O−H appeared at 989 cm^{-1} in PDPPA.[27] It was observed to be shifted to 981 cm^{-1} in EDOT-PDPPA confirms the interaction of the lone pair of P−O with EDOT. The characteristic assym (C═C) stretching band of EDOT observed at 1452 cm^{-1} is shifted to 1446 cm^{-1} in EDOT-PDPPA. The band maxima measured at 978 cm^{-1} in EDOT of C−S were observed to be shifted to 889 cm^{-1} in EDOT-PDPPA.[21] These observed shifts in the characteristic bands of EDOT and PDPPA in the FTIR spectrum of EDOT-PDPPA reveal the presence of various types of molecular interactions between these two molecules during the formation of the adduct. EDOT-PDPPA can form self-assembled supramolecular architectures through various interactions such as Coulombic forces among hydrophilic cations (phosphonium $^{\delta+}$) and anions (thiophene$^{\delta-}$) present in the ionic head groups and also form interdigitated self-assembled structure via antiparallel stacking of the hydrophobic alkyl chains through electrostatic layer by layer assembling.

Investigation on the lyotropic phase formation of EDOT-PDPPA in water was performed by observation under PLM. At low concentration of EDOT-PDPPA in water, the molecular layers of EDOT-PDPPA with the hydrophilic head and hydrophobic tails are randomly oriented and no distinct texture was observed, revealing the formation of the isotropic phase. On increasing concentration, individual molecules loss their degree of freedom partially and self-assemble by means of ion−dipole interaction between the ionic head regions and layer by layer interdigitation of alkyl chains to form micelles. The CMC of the EDOT-PDPPA in water was determined using UV−vis absorption measurements as 5×10^{-4}. On further increasing the concentration of EDOT-PDPPA, various micelles undergo collision, and later they reorganized to form thermodynamically stable phases in water. These supramolecular assemblies are thermodynamically stable and may take the shape of the nematic gyroid (Figure 2A).

Gyroid type phase formation may be attributed to the strong intermolecular interaction among the charged ions present in the head groups, hydrophobic tails, and also inter planar $\pi-\pi$ stacking. On further increasing the concentration of molecular chains, their ordering in a particular direction, position, and orientation from the director angle changes, leading to another type of defects in the texture to form two dimensionally ordered columnar mesophases (Figure 2B). Here, approaching of molecular assemblies to close proximity is prevented by the repulsive interactions between the polar end groups, leaving nanochannels in between the columns. However, columnar layers are biaxially oriented, and the molecular layers in this phase are perpendicular to the layer planes. On further increasing the concentration of molecular chains, lamellar phases with more ordering were observed. Formation of multiple mesophase by increasing the number of molecular chains resulted from the frustration experienced by the gyroid shell during the transition from nematic to columnar to lamellar phases. The interdigitated bilayers are formed by the "EDOT-PDPPA" ensembles as shown in Scheme 1.

Formations of various LC phases were further confirmed by XRD analysis as shown in Figure 3. It showed a *d*-spacing of

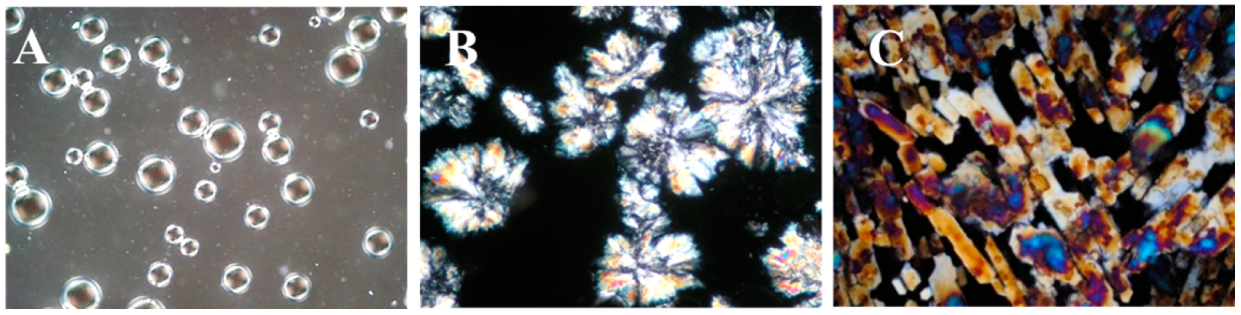

Figure 2. PLM images of EDOT-PDPPA: (A) nematic gyroid; (B) columnar; (C) lamellar.

DOI: 10.1021/acsami.5b04916
ACS Appl. Mater. Interfaces 2015, 7, 18028−18037

Scheme 1. Electrochemical Polymerization of Liquid Crystalline EDOT-PDPPA

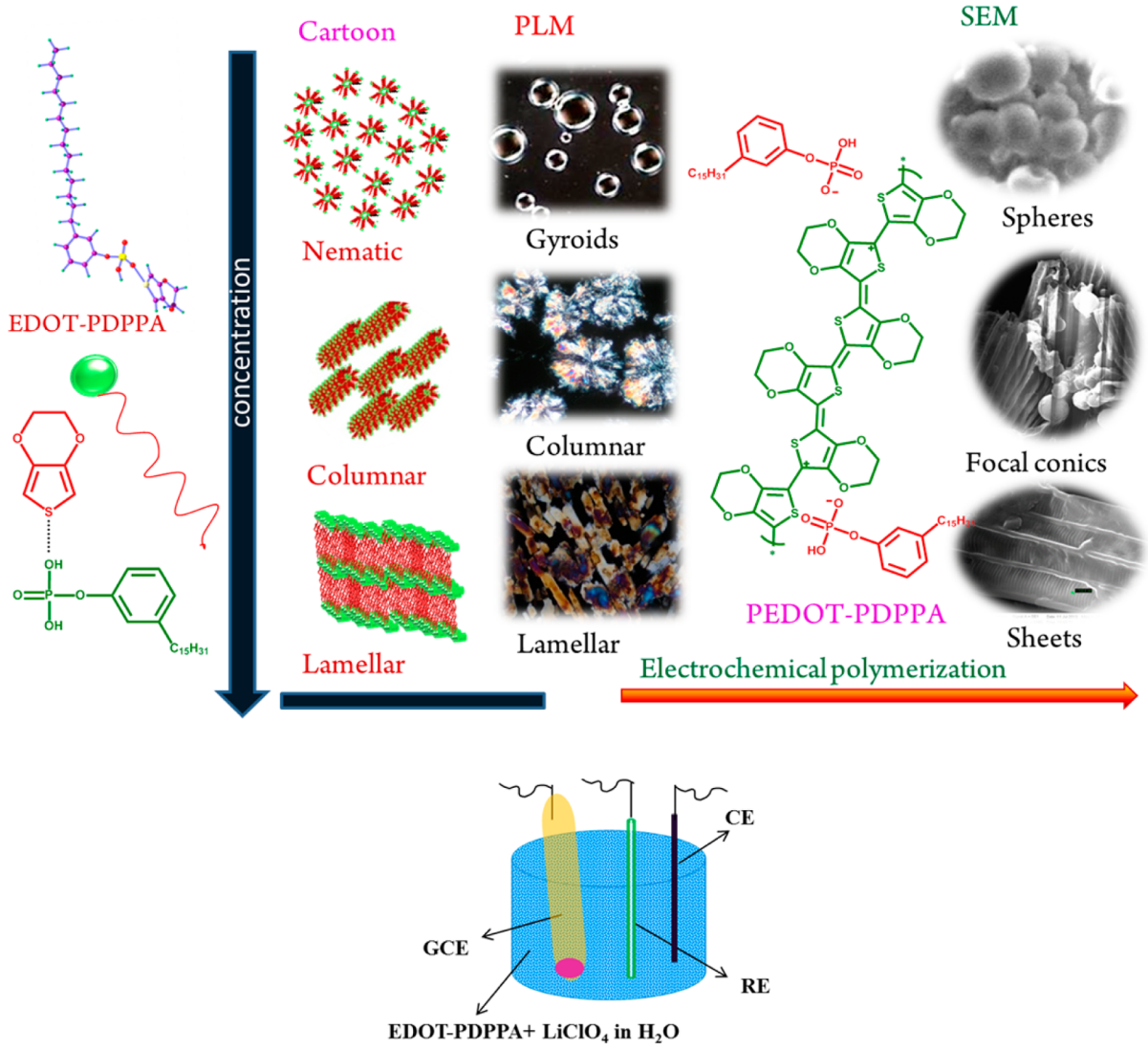

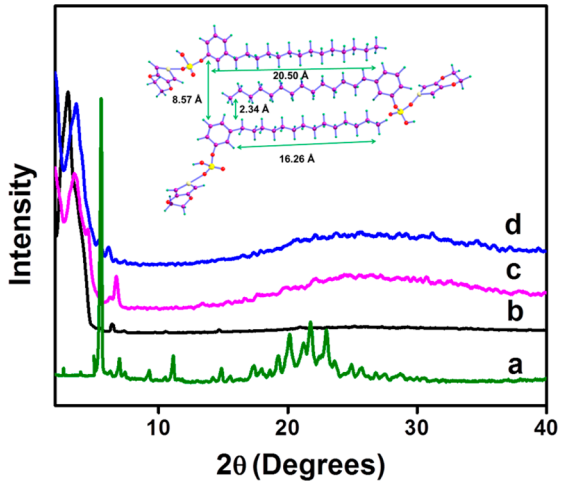

Figure 3. XRD of (a) PDPPA and (b) nematic, (c) lamellar, and (d) columnar phases of EDOT-PDPPA.

~37.35 Å, which is slightly less than twice the molecular length of "EDOT-PDPPA", suggesting the presence of interdigitated molecular layers in the supramolecular aggregates. The layer by layer self-assembled structure of EDOT PDPPA is given in the inset of Figure 3.

The XRD patterns of PDPPA and EDOT-PDPPA/water (nematic, columnar, and lamellar phase) are shown in Figure 3a to 3d, respectively. The XRD diagram of PDPPA exhibited well-defined sharp peak at 2θ = 5.5°, 6.97°, 9.28°, 20.13°, 21.73°, and 22.97° with *d*-spacing ~15.77, 12.66, 9.51, 4.40, 4.08, and 3.86 Å, revealing the formation of well-defined ordering in the crystalline phase. The XRD pattern of EDOT-PDPPA in the nematic phase exhibited a well-defined sharp intense peak at 2θ = 2.99° with *d*- spacing of ~29.61 Å, corresponding to the distance of the monodimensionally oriented layers. Diffractograms of EDOT-PDPPA cast from the columnar phase showed well-defined peaks at 2θ = 3.44° and 2θ = 6.75° (weak peak) with *d*-spacing of ~25.66 Å and ~13.09 Å. This *d*-spacing is slightly higher than the distance between the head groups and also the length of the repeating alkyl chain. This confirms the formation of a mesophase with hexagonal columnar symmetry. The XRD diagram of EDOT-PDPPA in the lamellar phase exhibited a sharp peak at 2θ = 3.64° with a *d*-spacing of ~24.29 Å and a small peak at 2θ = 6.15° with a *d*-spacing of ~14.39 Å, which is slightly higher than the length of the alkyl chain. As the concentration of EDOT-

DOI: 10.1021/acsami.5b04916
ACS Appl. Mater. Interfaces 2015, 7, 18028−18037

PDPPA increased, the distance between the hexagonal columns decreases and they pack more densely and merge to form more ordered layered lamellar phases with interdigitated hydrophobic bilayer (Figure 2C). These observations were supported by the studies made by other researchers, and they reported that LCs could exhibit different textures which depend upon the molecular shape, effect of surface alignment, and topological defect arising from the variations in the molecular organizations.[35,36] Thus, the formation of various mesophases such as nematic gyroid, columnar, and lamellar phases with characteristic textures observed in the EDOT-PDPPA/water system could generate well-defined channels and is expected to act as an intrinsic template for the formation of highly ordered PEDOT on the surface of GCE. The effect of these various LC phases on the morphology and electrochemical band gap and impedance is discussed below.

Characterization of PEDOT Patterned GCE. GCE was patterned through electrochemical polymerization of intrinsic liquid crystalline templates of EDOT-PDPPA/water in nematic, columnar, and lamellar phases and is shown in Scheme 1. The consecutive CVs observed during the electrochemical polymerization of EDOT-PDPPA in different LC phases with $LiClO_4$ on GCE when scanned between −0.2 and 0.85 V vs Ag/AgCl electrode are shown in Figure 4, and S1A and S1B. It has been

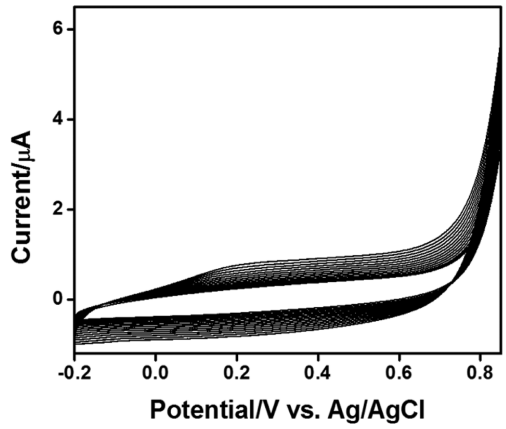

Figure 4. Cyclic voltammogram of electropolymerization of EDOT-PDPPA (lamellar phase).

observed that during the polymerization, when the liquid crystalline phase changed from nematic to hexagonal columnar to lamellar, the measured current increased from 33.89 μA to 40.11 μA to 57.89 μA, respectively, and the oxidation potential also showed variation in the potential at the current maxima from 0.85, 0.83, and 0.81 V. PEDOT films formed were found to be homogeneous and adherent to the electrode surface of GCE.

The chemical structure of the prepared PEDOT-PDPPA was confirmed by FT-IR spectroscopy. The FTIR spectra of PEDOT-PDPPA are shown in Figure 1. PEDOT-PDPPA exhibited peaks at 1520 and 1331 cm^{-1} which can be ascribed to the C−C and C═C stretching vibrations of the thiophene ring. The observed band maxima at 1197 and 1122 cm^{-1} are due to the C−O−C bond stretch in the ethylenedioxy group. The peaks at 980, 924, and 838 cm^{-1} are assigned to the thiophene C−S bond stretching. The peak observed at 1051 cm^{-1} is associated with the stretching vibrations in the ethylenedioxy group. The peak at 1746 cm^{-1} is associated with the doped level of PEDOT. The peaks observed at 2925 and 2853 cm^{-1} are ascribed to the characteristic $-CH_2-$ stretching of the ethylenedioxy bridge. The peaks at 635, 573, and 520 cm^{-1} are due to the stretching vibrations of O−P−O and O═P−O of ($-PO_4$). It was also observed that the peaks at 1398 cm^{-1} are related to −P═O. These results suggested that PEDOT is effectively doped with PDPPA. The presence of phosphorus in PEDOT-PDPPA was further confirmed by the EDX analysis.

The morphology of the PEDOT films prepared from liquid crystalline templates of EDOT-PDPPA in nematic, columnar, and lamellar phases was studied by PLM and SEM analysis. The SEM picture of PEDOT-PDPPA prepared from the nematic gyroid phase exhibited nanospheres (Figure 5A) while PEDOT synthesized from columnar phases exhibited columns or a web of peacock-like features in SEM (Figure 5B). The morphology of PEDOT prepared from the lamellar phase of EDOT-PDPPA exhibited a tubular/sheet-like morphology (Figure 5C and D). PLM images of NPEDOT, CPEDOT, and LPEDOT are shown in Figure S2A−C. An interesting observation made during morphological analysis is that PEDOT-PDPPA copycatted the liquid crystalline features of the monomer "EDOT-PDPPA". Under PLM, it showed birefringent spheres, columns, and lamellar textures for PEDOT-PDPPA prepared from LC templates of gyroid, columnar, and lamellar phases, respectively. These observations were further supported by the studies made by other researchers.[37−39] In the propagation step, PEDOT aggregates which are in the lyotropic mesophase may lose molecular order on a nanometer scale due to the thermodynamic influence of the growing chain. They form thermodynamically stable mesophases of inherent nanoscale dimensions via a self-assembly process. Similar observations were made by O'Brien et al.[40] They successfully prepared varieties of liquid crystalline assemblies with the preservation of the shape of the mesostructures of the monomers.

Further, the presence of phosphorus in PEDOT-PDPPA was confirmed by EDX analysis (Figure 5E). It showed a pattern containing the presence of carbon, sulfur, and phosphorus, and PEDOT prepared without template did not exhibit the presence of phosphorus (Figure 5F).

Studies on the Electrochemical Band Gap of PEDOT-PDPPA Modified GCE. The electrochemical band gaps of PEDOT-PDPPAs were calculated from the voltage difference of reduction (addition of an electron to the lowest unoccupied molecular orbital, LUMO) or oxidation (addition of a hole or removal of an electron from the highest occupied molecular orbital, HOMO).[41,42] HOMO−LUMO values for NPEDOT and CPEDOT were calculated by cyclic voltammetry, and the same are given in Figure S3. The cartoon showing various specific modes of ordering of the molecular layers in lamellar, columnar, and nematic liquid crystalline phases with the HOMO values measured by CV and the changes in the interlayer distance measured from XRD is shown in Table S1. The extent of ordering is in the order lamellar > columnar > nematic. As the ordering increases, the interlayer distance between the molecules decreases, which allows easier hopping of the charge carriers, and it also may show a surge in the motion of the charge carriers. Kasha et al. experimentally measured the changes in the HOMO−LUMO value during polymer assembling.[43] The HOMO values are as follows for NPEDOT (−5.04) to CPEDOT (−4.94) and LPEDOT (−4.89 eV) and the LUMO values for NPEDOT (−3.82 eV) to CPEDOT (−3.84 eV) and LPEDOT (−3.88 eV), respectively. The band gap calculated from electrochemical

DOI: 10.1021/acsami.5b04916
ACS Appl. Mater. Interfaces 2015, 7, 18028−18037

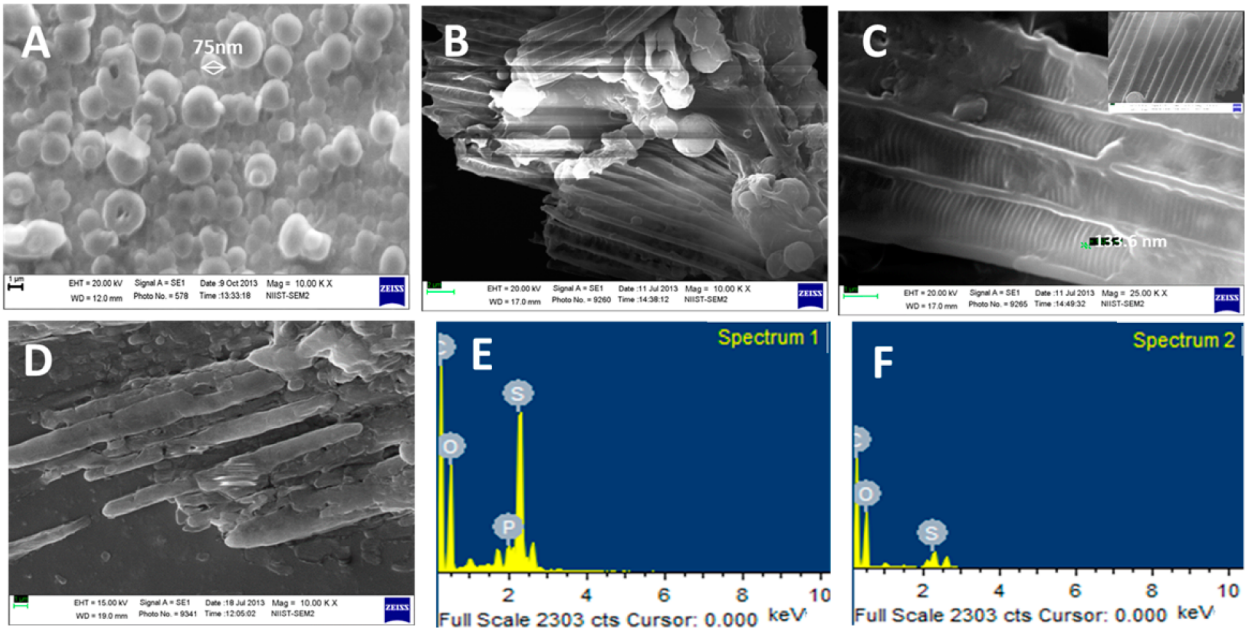

Figure 5. SEM images of PEDOT-PDPPA (A) nanospheres, (B) columns, (C) sheets (magnified image is shown in the inset), and (D) cylindrical tubes. EDX plots (E) of PEDOT-PDPPA and (F) PEDOT.

studies showed that the band gap is found to be decreasing from NPEDOT (1.22 eV), to CPEDOT (1.2 eV), to LPEDOT (1.01 eV), which confirmed the highly conducting nature of LPEDOT compared with NPEDOT and CPEDOT.

Electrochemical Impedance Spectroscopic Studies. Electrochemical impedance spectroscopy (EIS) is a non-destructive steady-state technique useful to probe electron transfer and electrical properties of surface modified electrodes and the mechanism of the charge conduction process at the electrode/electrolyte interface by applying an oscillating potential as a function of frequency in the redox probe $Fe(CN)_6^{3-/4-}$. The complex impedance (Z) can be presented as a sum of the real impedance ($Z'(\Omega)$) and the imaginary impedance ($Z''(\Omega)$), which are components that originate mainly from the resistance and capacitance of the cell.[44,45]

$$Z = Z' - iZ''$$

The typical electrochemical impedance spectrum can be presented in the form of Nyquist plots, Z'' vs Z', which are recorded as a function of frequency.

$$|Z| = [(Z')^2 + (Z'')^2]^{1/2}$$

A typical Nyquist plot includes a semicircle region lying on the Z'' axis followed by a straight line. The straight line in the lower frequency region represents the characteristics of the diffusion-limited electron transfer process between the electrode and electrolyte, and the semicircles at higher frequencies correspond to the electron transfer kinetics.[46] Figure 6A represents Nyquist plots for GCE, PEDOT/GCE, NPEDOT/GCE, CPEDOT/GCE, and LPEDOT/GCE. The equivalent circuit diagram is shown in Figure 6B, which is composed of the solution resistance (R_S), the constant phase element (CPE, Q), the electron transfer resistance (R_{et}), and the Warburg impedance (W) resulting from the diffusion of charged species from the bulk solution to the interphase. Due to the inhomogeneity of the electrode surface resulting from polymer films formed, CPE was used instead of an ideal double layer capacitance (C_{dl}) to take the depressed semicircles into

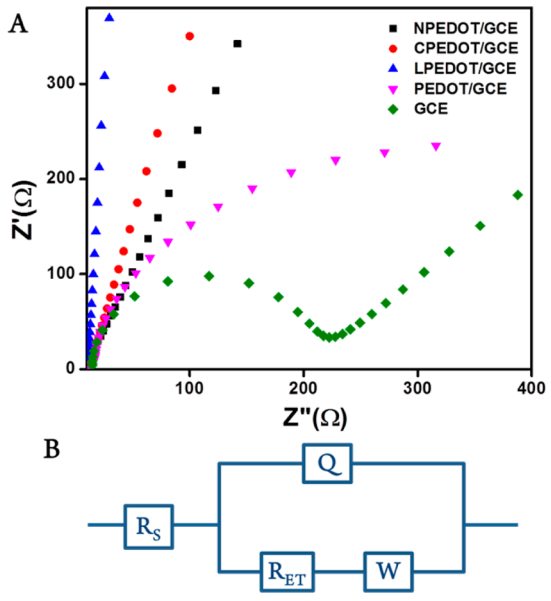

Figure 6. (A) Nyquist plots of (◆) GCE, (▼) PEDOT/GCE, (■) NPEDOT/GCE, (●) CPEDOT/GCE, and (▲) LPEDOT/GCE; (B) Equivalent circuit.

account. R_S is usually independent of composition changes, as it represents the bulk properties of the electrolyte solution.

PEDOT/GCE exhibited a straight line with a very small depressed semicircle area, and the electron transfer resistance of 101.3 Ω revealed that PEDOT accelerates the electron transfer rate and provides a network structure. The electron transfer resistance (R_{et}) values of NPEDOT/GCE, CPEDOT/GCE, and LPEDOT/GCE are measured as 95.67, 83, and 68.34 Ω, respectively. It has been observed that the anisotropic lamellar phase of LPEDOT exhibited a lower value of electron transfer resistance; otherwise, it exhibited a higher value of electron transfer conductance. This arises from the high extent of ordering with well-defined textures and domains, which could

DOI: 10.1021/acsami.5b04916
ACS Appl. Mater. Interfaces 2015, 7, 18028−18037

provide frisky channels for the transfer of electrons, and hence, the electron transfer conductance increased. The bulk anion, i.e. phosphonium ion, present in LPEDOT, tightly incorporated into the polymer matrix, induces internal capacitance for all the NPEDOT/GCE, NPEDOT/GCE, and LPEDOT/GCE.

Detection of Nicotine. The efficiency of the patterned transducer was studied by using it as a sensor for the detection of nicotine. From the above results, it has been observed that LPEDOT/GCE exhibited a low value of R_{et}, and hence, it is taken as a model electrode for studying the performance of the transducer. The electrocatalytic performance of LPEDOT/GCE in the electrochemical oxidation of nicotine was studied by both cyclic voltammetry and square wave voltammetry (SWV) in BR buffer (pH 8.0). The CV diagram showing the oxidation of nicotine (10^{-3} M) at the bare GCE and LPEDOT/GCE in the presence of nicotine in BR buffer (pH 8.0) at the scan rate of 0.05 V/s is given in Figure S4. At the bare GCE, CV exhibited a poorly resolved oxidation signal, and the peak is diffused over a broad potential region with a weak current response. When LPEDOT/GCE was replaced as the working electrode, the oxidation potential was observed as a well resolved peak at about 0.83 V with a peak current of 56.07 μA. The peak potential was shifted to the lower positive value as compared to bare GCE (+1.1 V), indicating electrocatalytic oxidation of nicotine. CVs were recorded at various scan rates from 0.01 V/S to 0.1 V/s in 1 mM nicotine in BR buffer solution (pH 8.0), and are shown in Figure 7. The plot of peak

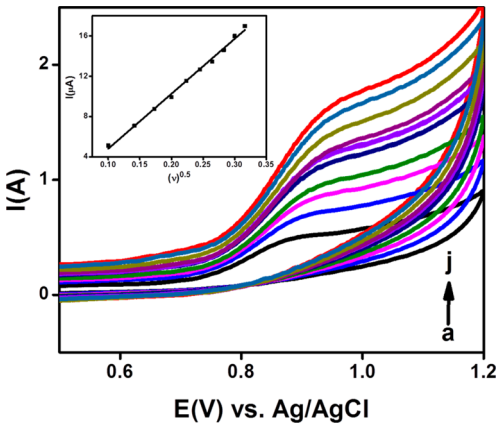

Figure 7. Effect of the scan rate on the CV responses of the LPEDOT/GCE (a) 0.01; (b) 0.02; (c) 0.03; (d) 0.04; (e) 0.05; (f) 0.06; (g) 0.07; (h) 0.08; (i) 0.09; and (j) 0.1 V/s in BR buffer with 1 mM nicotine. Plot of the square root of the scan rate vs the peak current is shown in the inset.

current vs the square root of scan rates, exhibiting a straight line with a good linear response (regression coefficient $R^2 > 0.99$), revealed the oxidation process of nicotine at the modified electrode is diffusion controlled.[47] The oxidation of nicotine was studied at NPEDOT/GCE and CPEDOT/GCE (Figure S4c and d). The peak corresponding to the nicotine oxidation was observed to be 31.09 μA and 39.90 μA at NPEDOT/GCE and CPEDOT/GCE, respectively, which were lower than that of LPEDOT/GCE. Hence, further studies were carried out with LPEDOT/GCE.

Square wave voltammetry (SWV) was also used for studying the electrocatalytic performance of LPEDOT/GCE for the oxidation of nicotine. In SWV, the peaks in the differential current vs applied potential were used instead of separate forward and reverse current plots. So significant time evolution between potential reversal and current sampling, high sensitivity screening can be obtained, since the background currents may be suppressed much more effectively than CV. The SWV response of LPEDOT/GCE after the addition of nicotine in BR buffer solution showed a clearly resolved oxidation peak at 0.83 V (Figure 8). The peaks in the plots are indicative of a redox process, and the magnitudes of the peaks are proportional to the concentrations of various redox active species. Figure 8 shows the well resolved SWV obtained during the successive additions of nicotine in BR buffer solution (pH 8.0). LPEDOT/GCE exhibited a linear relationship with nicotine in the concentration range of 0.1 μM to 320 μM, and the limit of detection of nicotine was calculated as 50 nM.

Since the current response of the analyte is associated with the pH of the electrolyte solution, the SWV response of LPEDOT/GCE was studied by performing experiments by varying pH. Investigation on the peak potential (E_p) and peak current (I_p) of nicotine was done by SWV in the pH range from 2 to 12 using BR buffer solutions. The effect of pH on the peak current (I_p) of nicotine in the range of pH 2−12 is showed in Figure 9. With an increase of from pH 6 to 8, an enhancement of peak current was observed. On increasing the pH, the peak current tends to decrease and remains almost a constant value. Hence, pH 8 is selected as the finest composition of the buffer for the sensing of nicotine. At acidic pH (2 to 5), the current response of nicotine was barely visible with magnitudes close to the blank. Nevertheless, it was found that the oxidation peak of nicotine shifted toward lower positive potentials with the increase of pH from 6 to 12, indicating proton participation in the oxidation reaction as the suggested mechanism by Suffredini et al.[48] They studied the oxidation of nicotine in alkaline media at a boron-doped diamond electrode. Nicotine is a weak diacidic base with two pK_a values at pK_{a1} (3.12) and pK_{a2} (8.02) which correspond to the protonation of the diprotonated pyridine nitrogen and monoprotonated pyrrolidine nitrogen present in nicotine. The first intersection point observed at pH 8.0 was close to pK_{a2}, as a result of the changes of the protonation of the nitrogen in the pyrrolidine moiety. At pH 9−12 the unprotonated form of nicotine predominates and no proton transfer occurs in the rate-determining step. These results strongly indicated that the oxidation site of nicotine is situated on the pyrrolidine ring and ascribed to the oxidation of tertiary nitrogen.

We have made a comparative performance of the LPEDOT/GCE with the literature,[47−58] and the results are given in Table S2. Studies showed that LPEDOT/GCE exhibited high sensitivity and lower detection limit than the reported methods.

The selectivity of LPEDOT/GCE transduced on nicotine was evaluated by adding possible interfering substances such as glucose, dopamine, ascorbic acid, tyrosine, and uric acid to 50 μM nicotine under optimized conditions. It has been observed that these substances could not make any alteration in the measured values of the oxidation potential or current of nicotine under study.

To validate the applicability of the proposed method for the determination of nicotine in real samples, recovery experiments were performed under optimized SWV at LPEDOT/GCE. Three brands of commercially available cigarettes (C1, C2, and C3) were analyzed, and the values are given in Table 1. Recoveries ranged from 94.09 to 101.24% for C1 sample, 97.27 to 102.27% for C2 sample, and 99.27 to 102.23% for C3 sample, respectively. These results suggested that the proposed

DOI: 10.1021/acsami.5b04916
ACS Appl. Mater. Interfaces 2015, 7, 18028−18037

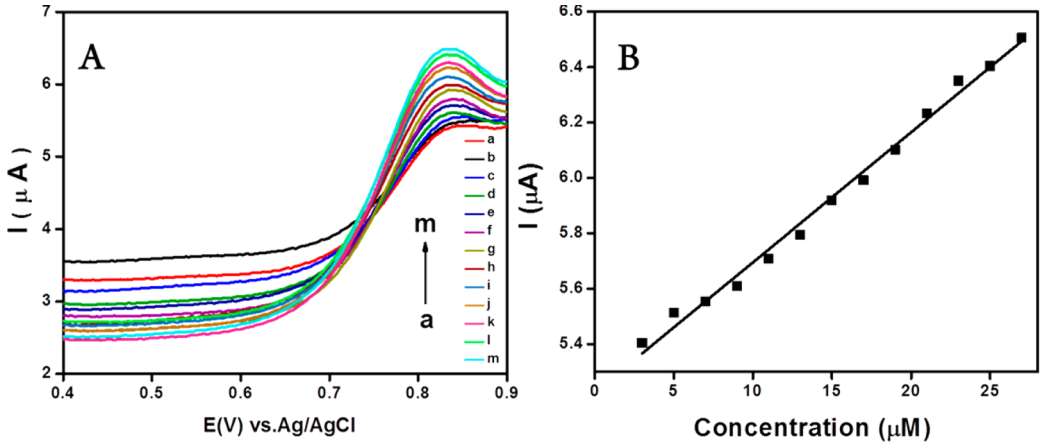

Figure 8. (A) Effect of the nicotine concentration on the SWV responses of the modified electrode in BR buffer (pH 8.0): (a) 0.3 μM, (b) 0.5 μM, (c) 0.7 μM and (d) 0.9 μ M, (e) 1.1 μM, (f) 1.3 μM, (g) 1.5 μM, (h) 1.7 μM, (i) 1.9 μM, (j) 2.1 μM, (k) 2.3 μM, (l) 2.5 μM, and (m) 2.7 μM nicotine. (B) Linear relationship of peak current with respect to concentration.

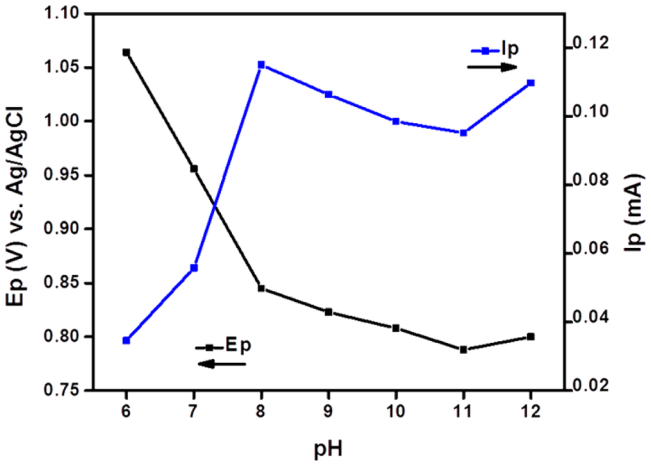

Figure 9. Effect of pH on peak current Ip and peak potential Ep.

method is suitable and satisfactorily accurate for the quantification of nicotine in cigarettes.

CONCLUSIONS

We have patterned glassy carbon electrode with well-ordered predesigned nanostructured PEDOT through electrochemical polymerization of a biobased liquid crystalline template (EDOT-PDPPA). Self-assembled "EDOT-PDPPA" in water exhibited concentration dependent liquid crystalline phases of "nematic gyroid", "columnar" and "lamellar" phases. During electrochemical polymerization, PEDOTs preserved and locked the ordering of the LC template of the EDOT-PDPPA in the nanometer regime. The electrochemical properties of patterned GCE exhibited enhanced electrochemical charge conductance with low band gap compared to the one modified without template. Further, the modified electrode behaved as an electrochemical transducer for the detection of nicotine by CV and square wave voltammetry at a nanomolar level. Selectivity, interference, recovery, and real sample analysis were performed. This simple low cost strategy of electrochemical patterning of a conductive polymer with a desired ordering on the nanometer scale on the conventional electrode can be exploited for anode modifications which will fetch applications in various miniaturized plastronic devices.

ASSOCIATED CONTENT

Supporting Information

The Supporting Information is available free of charge on the ACS Publications website at DOI: 10.1021/acsami.5b04916.

Experimental procedure for the preparation of 3-pentadecyl phenyl phosphoric acid, PLM images of liquid crystalline polymers, CVs of electropolymerization, HOMO−LUMO studies and nicotine oxidation on various LC modified electrodes, and comparison of analytical methods for nicotine sensing available in the literature (PDF)

AUTHOR INFORMATION

Corresponding Author

*E mail: sudhajd2001@yahoo.co.in.

Table 1. Quantitative and Recovery Analysis of Nicotine in Cigarettes (n = 3)

cigarette sample	total nicotine content (w/w%) ± SD	determined (μM)	added (μM)	found (μM)	% recovery (mean ± % RSD)
C1	1.35 ± 0.04	20.56	50	66.39 ± 1.53	94.09 ± 2.16
			70	87.82 ± 2.51	96.97 ± 2.95
			100	128.13 ± 2.19	101.24 ± 3.22
C2	1.14 ± 0.02	18.94	50	67.06 ± 3.37	97.27 ± 4.42
			70	90.96 ± 2.98	102.27 ± 2.87
			100	117.31 ± 3.64	98.26 ± 3.39
C3	1.51 ± 0.01	24.62	50	75.95 ± 2.83	101.78 ± 3.72
			70	93.93 ± 3.96	99.27 ± 4.13
			100	127.41 ± 4.09	102.23 ± 3.21

DOI: 10.1021/acsami.5b04916
ACS Appl. Mater. Interfaces 2015, 7, 18028−18037

Notes

The authors declare no competing financial interest.

■ ACKNOWLEDGMENTS

We are thankful to A. Ajayaghosh, Director, CSIR-NIIST, Trivandrum, and Vijayamohanan K Pillai, Director, CSIR-CECRI, for constant encouragement and support. We are also thankful to Lucy Paul and Kiran Mohan for SEM and TEM analyses. We are also thankful for the financial support from CSIR network project MULTIFUN (CSC0101), NWP-54 and CSIR-SRF fellowship.

■ REFERENCES

(1) Heeger, A. J. Semiconducting Polymers: the Third Generation. *Chem. Soc. Rev.* **2010**, *39*, 2354−2371.
(2) Hatchett, D. W.; Josowicz, M. Composites of Intrinsically Conducting Polymers as Sensing Nanomaterials. *Chem. Rev.* **2008**, *108*, 746−769.
(3) Wang, W.; Ruderer, M. A.; Metwalli, E.; Guo, S.; Herzig, E. M.; Perlich, J.; Müller-Buschbaum, P. Effect of Methanol Addition on the Resistivity and Morphology of PEDOT:PSS Layers on Top of Carbon Nanotubes for Use as Flexible Electrodes. *ACS Appl. Mater. Interfaces* **2015**, *7*, 8789−8797.
(4) Kanibolotsky, A. L.; Perepichka, I. F.; Skabara, P. J. Star-shaped [small pi]-conjugated Oligomers and Their Applications in Organic Electronics and Photonics. *Chem. Soc. Rev.* **2010**, *39*, 2695−2728.
(5) Wei, W.; Wang, H.; Hu, Y. H. A Review on PEDOT-based Counter Electrodes for Dye-Sensitized Solar Cells. *Int. J. Energy Res.* **2014**, *38*, 1099−1111.
(6) Yoon, H.; Chang, M.; Jang, J. Formation of 1D Poly(3,4-ethylenedioxythiophene) Nanomaterials in Reverse Microemulsions and Their Application to Chemical Sensors. *Adv. Funct. Mater.* **2007**, *17*, 431−436.
(7) Musumeci, C.; Hutchison, J. A.; Samori, P. Controlling the Morphology of Conductive PEDOT by in situ Electropolymerization: from Thin Films to Nanowires with Variable Electrical Properties. *Nanoscale* **2013**, *5*, 7756−7761.
(8) Mukherjee, S.; Singh, R.; Gopinathan, S.; Murugan, S.; Gawali, S.; Saha, B.; Biswas, J.; Lodha, S.; Kumar, A. Solution-Processed Poly(3,4-ethylenedioxythiophene) Thin Films as Transparent Conductors: Effect of p-Toluenesulfonic Acid in Dimethyl Sulfoxide. *ACS Appl. Mater. Interfaces* **2014**, *6*, 17792−17803.
(9) Tsakova, V.; Winkels, S.; Schultze, J. W. Anodic Polymerization of 3,4-ethylenedioxythiophene from Aqueous Microemulsions. *Electrochim. Acta* **2001**, *46*, 759−768.
(10) Iyoda, T.; Ando, M.; Kaneko, T.; Ohtani, A.; Shimidzu, T.; Honda, K. Electron Microscopic Evidence for the Layered Structure of A Conducting Polypyrrole Langmuir-Blodgett Film. *Langmuir* **1987**, *3*, 1169−1170.
(11) Bao, Z.; Rogers, J. A.; Katz, E. H. Printable Organic and Polymeric Semiconducting Materials and Devices. *J. Mater. Chem.* **1999**, *9*, 1895−1904.
(12) Brown, T. M.; Kim, J. S.; Friend, R. H.; Cacialli, F.; Daik, R.; Feast, W. J. Built-in Field Electroabsorption Spectroscopy of Polymer Light Emitting Diodes Incorporating A Doped Poly(3,4-ethylene dioxythiophene) Hole Injection Layer. *Appl. Phys. Lett.* **1999**, *75*, 1679−1681.
(13) Chen, S.; Li, Y.; Li, Y. Architecture of Low Dimensional Nanostructures Based on Conjugated Polymers. *Polym. Chem.* **2013**, *4*, 5162−5180.
(14) Babu, S. S.; Praveen, V. K.; Ajayaghosh, A. Functional π-Gelators and Their Applications. *Chem. Rev.* **2014**, *114*, 1973−2129.
(15) Fall, M.; Aaron, J. J.; Sakmeche, N.; Dieng, M. M.; Jouini, M.; Aeiyach, S.; Lacroix, J. C.; Lacaze, P. C. Electrochemical and Spectroscopic Properties of Poly(3-methoxythiophene) Electrosynthesized in An Aqueous Micellar Medium. *Synth. Met.* **1998**, *93*, 175−179.
(16) Luo, J.; Zhou, Q.; Sun, J.; Jiang, J.; Zhou, X.; Zhang, H.; Liu, X. Photoresponsive Water- Dispersible Polyaniline Nanoparticles through Template Synthesis with Copolymer Micelle Containing Coumarin Groups. *J. Polym. Sci., Part A: Polym. Chem.* **2012**, *50*, 4037−4045.
(17) Lu, C.; Ben, T.; Xu, S.; Qiu, S. Electrochemical Synthesis of A Microporous Conductive Polymer Based on A Metal−Organic Framework Thin Film. *Angew. Chem., Int. Ed.* **2014**, *53*, 6454−6458.
(18) Dobretsova, L. Y.; Ermolaev, S. V.; Milinchuk, V. K.; Jitariouk, N. I.; Le Moel, A. Structure of Conducting Polymer Films Prepared on the Surface and in the Pores of Poly(ethylene terephthalate) Track Membranes by Template Synthesis. *High Energy Chem.* **2005**, *39*, 361−367.
(19) Sudha, J. D.; Sivakala, S.; Chandrakanth, C. K.; Neethu, K. S.; Rohini, K. N.; Ramakrishnan, R. Percolated Conductive Polyaniline-Clay Nanocomposite in Polyvinyl Chloride through the Combined Approach Porous Template and Self-Assembly. *eXPRESS Polym. Lett.* **2014**, *8*, 107−115.
(20) Hulvat, J. F.; Stupp, S. I. Liquid-Crystal Templating of Conducting Polymers. *Angew. Chem., Int. Ed.* **2003**, *42*, 778−781.
(21) Devaki, S. J.; Sadanandhan, N. K.; Sasi, R.; Adler, H.-J. P.; Pich, A. Water Dispersible Electrically Conductive Poly(3,4-ethylenedioxythiophene) Nanospindles by Liquid Crystalline Template Assisted Polymerization. *J. Mater. Chem. C* **2014**, *2*, 6991−7000.
(22) Hatano, T.; Bae, A.-H.; Takeuchi, M.; Fujita, N.; Kaneko, K.; Ihara, H.; Takafuji, M.; Shinkai, S. Helical Superstructure of Conductive Polymers as Created by Electrochemical Polymerization by Using Synthetic Lipid Assemblies as a Template. *Angew. Chem.* **2004**, *116*, 471−475.
(23) Han, M. G.; Foulger, S. H. Facile Synthesis of Poly(3,4-ethylenedioxythiophene) Nanofibers from An Aqueous Surfactant Solution. *Small* **2006**, *2*, 1164−1169.
(24) Gök, A.; Omastová, M.; Yavuz, A. G. Synthesis and Characterization of Polythiophenes Prepared in the Presence of Surfactants. *Synth. Met.* **2007**, *157*, 23−29.
(25) Sakmeche, N.; Bazzaoui, E. A.; Fall, M.; Aeiyach, S.; Jouini, M.; Lacroix, J. C.; Aaron, J. J.; Lacaze, P. C. Application of Sodium Dodecylsulfate (SDS) Micellar Solution as An Organized Medium for Electropolymerization of Thiophene Derivatives in Water. *Synth. Met.* **1997**, *84*, 191−192.
(26) Sudha, J. D.; Reena, V. L.; Pavithran, C. Facile Green Strategy for Micro/Nano Structured Conducting Polyaniline-Clay Nanocomposite via Template Polymerization Using Amphiphilic Dopant, 3-Pentadecyl Phenol 4-Sulphonic Acid. *J. Polym. Sci., Part B: Polym. Phys.* **2007**, *45*, 2664−2673.
(27) Sudha, J. D.; Sasikala, T. S. Studies on the Formation of Self-Assembled Nano/Microstructured Polyaniline−Clay Nanocomposite (PANICN) Using 3-Pentadecyl Phenyl Phosphoric Acid (PDPPA) as A Novel Intercalating Agent cum Dopant. *Polymer* **2007**, *48*, 338−347.
(28) Wang, J. *Analytical Electrochemistry*; Wiley: 2006.
(29) Yildiz, D. Nicotine, Its Metabolism and An overview of Its Biological Effects. *Toxicon* **2004**, *43*, 619−632.
(30) Wilson, A. L.; Langley, L. K.; Monley, J.; Bauer, T.; Rottunda, S.; McFalls, E.; Kovera, C.; McCarten, J. R. Nicotine Patches in Alzheimer's Disease: Pilot Study on Learning, Memory, and Safety. *Pharmacol., Biochem. Behav.* **1995**, *51*, 509−514.
(31) Rezvani, A. H.; Levin, E. D. Cognitive Effects of Nicotine. *Biol. Psychiatry* **2001**, *49*, 258−267.
(32) Alberg, A. J. Cigarette Smoking: Health Effects and Control Strategies. *Drugs Today* **2008**, *44*, 895−904.
(33) Lakshmi, D.; Whitcombe, M. J.; Davis, F.; Sharma, P. S.; Prasad, B. B. Electrochemical Detection of Uric Acid in Mixed and Clinical Samples: A Review. *Electroanalysis* **2011**, *23*, 305−320.
(34) Seo, J.; Kim, S.; Gihm, S. H.; Park, C. R.; Park, S. Y. Highly Fluorescent Columnar Liquid Crystals with Elliptical Molecular Shape: Oblique Molecular Stacking and Excited-State Intramolecular Proton-Transfer Fluorescence. *J. Mater. Chem.* **2007**, *17*, 5052−5057.
(35) Mermin, N. D. The Topological Theory of Defects in Ordered Media. *Rev. Mod. Phys.* **1979**, *51*, 591−648.
(36) Revannasiddaiah, N. D.; Krishnamurti, D. Optical Behaviour of Mixtures of Nematic and Cholesteric Compounds. *Mol. Cryst. Liq. Cryst.* **1983**, *101*, 103−127.

DOI: 10.1021/acsami.5b04916
ACS Appl. Mater. Interfaces 2015, 7, 18028−18037

(37) Venkatesan, K.; Kouwer, P. H. J.; Yagi, S.; Muller, P.; Swager, T. M. Columnar Mesophases from Half-Discoid Platinum Cyclometalated Metallomesogens. *J. Mater. Chem.* **2008**, *18*, 400−407.
(38) Kruk, M.; Jaroniec, M.; Yang, Y.; Sayari, A. Determination of the Lamellar Phase Content in MCM-41 Using X-ray Diffraction, Nitrogen Adsorption, and Thermogravimetry. *J. Phys. Chem. B* **2000**, *104*, 1581−1589.
(39) Finklea, H. O.; Avery, S.; Lynch, M.; Furtsch, T. Blocking Oriented Monolayers of Alkyl Mercaptans on Gold Electrodes. *Langmuir* **1987**, *3*, 409−413.
(40) Fung, M. K.; Lai, S. L.; Tong, S. W.; Chan, M. Y.; Lee, C. S.; Lee, S. T.; Wu, W. W.; Inbasekaran, M.; O'Brien, J. J. Anode Modification of Polyfluorene-based Polymer Light-Emitting Devices. *Appl. Phys. Lett.* **2002**, *81*, 1497−1499.
(41) Xia, J.; Masaki, N.; Lira-Cantu, M.; Kim, Y.; Jiang, K.; Yanagida, S. Effect of Doping Anions' Structures on Poly(3,4-ethylenedioxythiophene) as Hole Conductors in Solid-State Dye-Sensitized Solar Cells. *J. Phys. Chem. C* **2008**, *112*, 11569−11574.
(42) Kiya, Y.; Hutchison, G. R.; Henderson, J. C.; Sarukawa, T.; Hatozaki, O.; Oyama, N.; Abruña, H. D. Elucidation of the Redox Behavior of 2,5-Dimercapto-1,3,4-thiadiazole (DMcT) at Poly(3,4-ethylenedioxythiophene) (PEDOT)-Modified Electrodes and Application of the DMcT−PEDOT Composite Cathodes to Lithium/Lithium Ion Batteries. *Langmuir* **2006**, *22*, 10554−10563.
(43) Kasha, M.; Rawls, H. R.; El-Bayoumi, M. A. *Pure Appl. Chem.* **1965**, *11*, 371−392.
(44) Randles, J. E. B. Kinetics of Rapid Electrode Reactions. *Discuss. Faraday Soc.* **1947**, *1*, 11−19.
(45) Barsoukov, E.; Macdonald, J. R. *Impedance Spectroscopy: Theory, Experiment, and Applications*; Wiley: 2005.
(46) Zhou, F.; Hu, H.; Yu, B.; Osborne, V. L.; Huck, W. T. S.; Liu, W. Probing the Responsive Behavior of Polyelectrolyte Brushes Using Electrochemical Impedance Spectroscopy. *Anal. Chem.* **2007**, *79*, 176−182.
(47) Švorc, L.; Stanković, D. M.; Kalcher, K. Boron-doped Diamond Electrochemical Sensor for Sensitive Determination of Nicotine in Tobacco Products and Anti-smoking Pharmaceuticals. *Diamond Relat. Mater.* **2014**, *42*, 1−7.
(48) Suffredini, H. B.; Santos, M. C.; De Souza, D.; Codognoto, L.; Homem-de-Mello, P.; Honório, K. M.; da Silva, A. B. F.; Machado, S. A. S.; Avaca, L. A. Electrochemical Behavior of Nicotine Studied by Voltammetric Techniques at Boron-Doped Diamond Electrodes. *Anal. Lett.* **2005**, *38*, 1587−1599.
(49) Hannisdal, A.; Mikkelsen, Ø.; SchrØder, K. H. Analysis of Nicotine in Antismoking Pharmaceutical Products by Differential Pulse Polarography and Voltammetry. *Collect. Czech. Chem. Commun.* **2007**, *72*, 1207−1213.
(50) Wu, C.-T.; Chen, P.-Y.; Chen, J.-G.; Suryanarayanan, V.; Ho, K.-C. Detection of Nicotine Based on Molecularly Imprinted TiO_2-Modified Electrodes. *Anal. Chim. Acta* **2009**, *633*, 119−126.
(51) Levent, A.; Yardim, Y.; Senturk, Z. Voltammetric Behavior of Nicotine at Pencil Graphite Electrode and Its Enhancement Determination in the Presence of Anionic Surfactant. *Electrochim. Acta* **2009**, *55*, 190−195.
(52) Wang, S.-J.; Liaw, H.-W.; Tsai, Y.-C. Low Potential Detection of Nicotine at Multiwalled Carbon Nanotube−Alumina-Coated Silica Nanocomposite. *Electrochem. Commun.* **2009**, *11*, 733−735.
(53) Highton, L.; Kadara, R. O.; Jenkinson, N.; Logan Riehl, B.; Banks, C. E. Metallic Free Carbon Nanotube Cluster Modified Screen Printed Electrodes for the Sensing of Nicotine in Artificial Saliva. *Electroanalysis* **2009**, *21*, 2387−2389.
(54) Xiong, H.; Zhao, Y.; Liu, P.; Zhang, X.; Wang, S. Electrochemical Properties and the Determination of Nicotine at A Multi-Walled Carbon Nanotubes Modified Glassy Carbon Electrode. *Microchim. Acta* **2010**, *168*, 31−36.
(55) Sims, M. J.; Rees, N. V.; Dickinson, E. J. F.; Compton, R. G. Effects of Thin-Layer Diffusion in the Electrochemical Detection of Nicotine on Basal Plane Pyrolytic Graphite (BPPG) Electrodes Modified with Layers of Multi-Walled Carbon Nanotubes (MWCNT-BPPG). *Sens. Actuators, B* **2010**, *144*, 153−158.
(56) Geto, A.; Amare, M.; Tessema, M.; Admassie, S. Voltammetric Determination of Nicotine at Poly(4-Amino-3-Hydroxynaphthalene Sulfonic Acid)-Modified Glassy Carbon Electrode. *Electroanalysis* **2012**, *24*, 659−665.
(57) Lo, T. W. B.; Aldous, L.; Compton, R. G. The Use of Nano-Carbon as An Alternative to Multi-Walled Carbon Nanotubes in Modified Electrodes for Adsorptive Stripping Voltammetry. *Sens. Actuators, B* **2012**, *162*, 361−368.
(58) Kassa, H.; Geto, A.; Admassie, S. Voltammetric Determination of Nicotine in Cigarette Tobacco at Electrochemically Activated Glassy Carbon Electrode. *Bull. Chem. Soc. Ethiop.* **2013**, *27*, 321−328.

DOI: 10.1021/acsami.5b04916
ACS Appl. Mater. Interfaces 2015, 7, 18028−18037